Hanle magnetoresistance: The role of edge spin accumulation and interfacial spin current

H. Wu, X. Zhang, C. H. Wan, B. S. Tao, L. Huang, W. J. Kong, and X. F. Han*

Beijing National Laboratory for Condensed Matter Physics, Institute of Physics, University of Chinese Academy of Sciences, Chinese Academy of Sciences, Beijing 100190, China

(Received 22 July 2016; revised manuscript received 21 September 2016; published 4 November 2016)

We report the Hanle magnetoresistance (HMR) due to the spin precession of edge spin accumulation and interfacial spin current. Because of spin-orbit coupling (SOC), an electric current is accompanied by a transverse spin current, which builds up the spin accumulation at surfaces of Pt and the spin current across the YIG/Pt interface. Once a magnetic field is applied, the precession of spins will decrease the edge spin accumulation and interfacial spin current, which leads to an increased resistance of Pt via ISHE. Spin relaxation governs the HMR from edge spin accumulation, while spin diffusion and spin conversion play important roles in the HMR from interfacial spin current. This work provides another method to investigate the spin-orbit coupling by electrical measurement.

DOI: 10.1103/PhysRevB.94.174407

Spin-orbit coupling (SOC) provides the possibility to couple spin and orbital degrees of freedom of electrons in conducting materials [1,2]. The resulting spin Hall effect (SHE) [3–5] and inverse spin Hall effect (ISHE) [6–8] can convert between spin and charge currents, where the ratio of spin and charge conductivities can be quantified by spin Hall angle (SHA) θ_{SH}. There are three mechanisms for SHE: intrinsic [9], skew scattering [10], and side-jump scattering [11]. Heavy metals are good candidates for SHE because θ_{SH} roughly follows a linear dependence on Z^4, where Z is the atomic number [12]. In particular, there are many studies on ferromagnet/heavy metal (FM/HM) bilayers, where the spin current in HM flows to the FM/HM interface. After spin memory loss [13] and spin back flow [14] at the interface, only a portion can be absorbed by FM via spin-transfer torque (STT) effect [15–17], which leads to a damping or antidamping torque on FM, and vice versa. Spin Hall-induced magnetization switching [18,19], spin pumping [6,20], and spin Hall magnetoresistance (SMR) [21–23] in FM/HM are all attributed to this interfacial spin current commutation between HM and FM.

Recently, a theoretical work predicted the Hanle magnetoresistance (HMR) effect in metals with strong SOC [24]. Electric current-induced edge spin accumulation is created on the scale of spin diffusion length due to SHE, mainly at top and bottom surfaces in thin film structures. When a magnetic field is applied in the direction perpendicular to the spin polarized direction, the spin begins to precess around the magnetic field via the Hanle effect, which would decrease the edge spin accumulation and then lead to an increase of the resistance by ISHE. In previous investigations of FM/HM structures, some parameters to quantify the strength of SOC such as spin Hall angle θ_{SH} and spin diffusion length λ span orders of magnitude for the same material by different groups, because the spin mixing conductance is very sensitive to the quality of the interface between FM and HM [25–27]. However, HMR induced by the spin precession of edge spin accumulation just needs a single HM layer without FM, which allows us to obtain the intrinsic parameters of SOC. Moreover, in FM/HM structures, besides conventional SMR which is related to the magnetization of FM, the spin precession of the edge spin accumulation and the spin current transport across the interface by a magnetic field will also generate an additional HMR contribution.

A recent experimental work reported the HMR in Pt on YIG and Pyrex substrates, and the HMR in Pyrex/Pt, was only observed at low temperature (100 K) [28]. However, HMR results from the intrinsic SOC in pure Pt. In principle, it should not depend on any other factors such as substrates and low temperature, and the signal-to-noise ratio needs also to be improved. So careful optimization of deposition conditions is an essential step toward future research. Furthermore, due to the open-circuit condition in Si-SiO_2/Pt, only the edge spin accumulation governs the HMR. While in YIG/Pt, apart from the edge spin accumulation, the additional spin current transport across the interface could also contribute to the HMR. The different roles of edge spin accumulation and interfacial spin current in HMR in these two systems should also be clarified, which is helpful to understand further spin transport and precession process.

Liquid-phase epitaxial 3.5-μm $Y_3Fe_5O_{12}$ (YIG) (111) films were prepared on 300-μm $Gd_3Ga_5O_{12}$ (GGG) (111) substrates, and then Pt films were deposited on Si-SiO_2 and GGG/YIG substrates by an ultrahigh vacuum magnetron sputtering system (ULVAC). The base pressure of the sputtering chamber was 1×10^{-7} Pa, and the Pt films were deposited at a low speed of 1 Å/s with a pressure of 0.06 Pa and a power of 120 W. Before deposition, an *in situ* 60-s etching by Ar plasma was carried out to clean the surface of substrates. The resistivity of the 5-nm Pt film on Si-SiO_2 and GGG/YIG at 300 K is 5.05×10^{-5} Ω cm and 4.08×10^{-5} Ω cm respectively. The Hall bar geometry of the film was fabricated by standard photolithography technique combined with Ar ion etching, and the size of the Hall bar is 100×1000 μm. The magnetic field $\boldsymbol{H}$ dependence of the magnetization $\boldsymbol{M}$ was measured by a vibrating sample magnetometer (VSM EZ-9, MicroSense). All magnetotransport measurements were performed in a physical property measurement system (PPMS-9T, Quantum Design) with a horizontal rotator option.

*xfhan@iphy.ac.cn

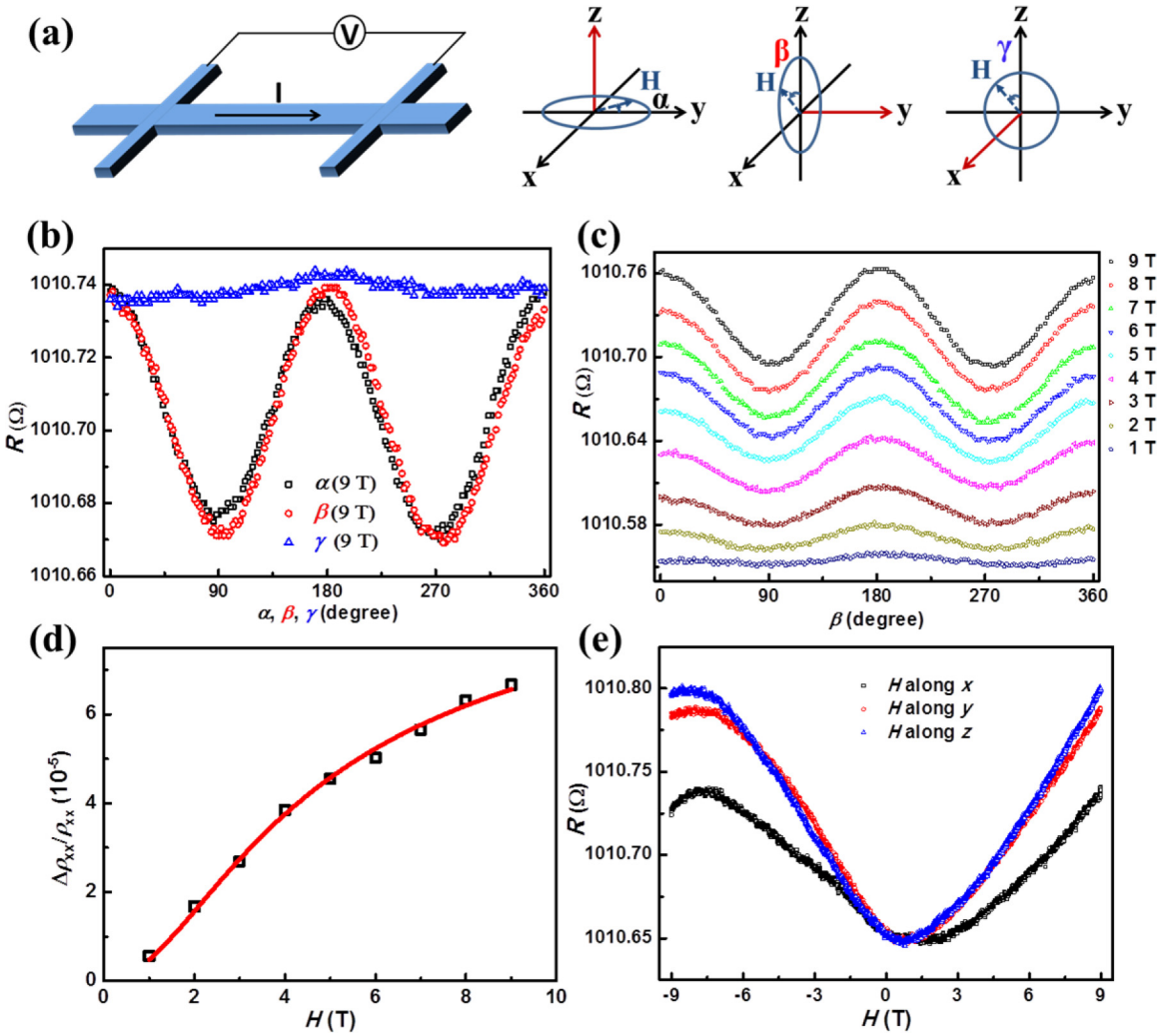

FIG. 1. (a) The schematic of the Hall bar geometry and the measurement setup, and the definitions of scanning angles α, β, and γ during the sample rotation at a constant magnetic field. Panels (b)–(e) were measured in Si-SiO_2/Pt (5 nm) sample at 300 K. (b) ADMR measurements with sample scanning in three planes (α, β, γ) at a 9-T magnetic field. (c) ADMR measurements at the magnetic field from 1 to 9 T. (d) The magnetic field dependence of normalized HMR, which is obtained from the amplitude of ADMR, and the fitting curve from Eq. (1) (red line). (e) *R*-*H* curves with magnetic field scanning from −9 to 9 T along *x*, *y*, and *z* directions.

Figure 1(a) shows the angular-dependent magnetoresistance (ADMR) measurement setup and the definitions of the scanning angles α, β, and γ during the sample rotation at a constant magnetic field. Due to SHE, the electric current J_e applied along the y direction during the ADMR measurement accompanies with a spin current J_S flowing in the z direction (perpendicular to the film plane) with x-directional spin polarization $\boldsymbol{\sigma}$, $J_S = \theta_{SH}\boldsymbol{\sigma} \times J_e$, and then the spin accumulation μ_S is created at top and bottom surfaces of Pt film. Hanle effect–induced resistance increase maximizes when magnetic field $\boldsymbol{H}$ is perpendicular to the spin polarization $\boldsymbol{\sigma}$, while no resistance changes for the parallel case. Under a constant 9-T magnetic field, the ADMR curves in Si-SiO_2/Pt(5 nm) sample at 300 K are shown in Fig. 1(b), ADMR of Si-SiO_2/Pt shows $\cos^2\alpha$ and $\cos^2\beta$ dependences, and no ADMR is observed under the same precision when scanning angle γ, which are in accordance with the HMR theory [24]. These ADMR properties can rule out the possible origin of ordinary magnetoresistance (OMR) for nonmagnetic metals which arises from the cyclic motion of electrons in a magnetic field due to the Lorentz force and depends on the relative angle between the electron velocity $\boldsymbol{v}$ and the magnetic field $\boldsymbol{H}$ [29,30].

We changed the magnetic field from 1 to 9 T during the ADMR measurement, as shown in Fig. 1(c). Then we obtained the amplitude of ADMR and calculated the normalized HMR $\Delta\rho_{xx}/\rho_{xx}$ in every magnetic field, and plotted the $\Delta\rho_{xx}/\rho_{xx}$-$H$ curve [Fig. 1(d)]. According to the HMR theory, the shape of the magnetoresistance curve can be described as the following equation [24]:

$$\Delta\rho/\rho = (\Delta\rho/\rho)_{H\to\infty}\left\{1 - \left[\frac{1+\sqrt{1+x^2}}{2(1+x^2)}\right]^{1/2}\right\}, \qquad (1)$$

where $x = \Omega\tau$, $\Omega = g\mu_B B/\hbar$ is the spin precession frequency (g is the Lande factor, $\hbar$ is the reduced Planck constant, and B is the magnetic field), and τ is the effective spin lifetime during which the spin polarization is destroyed. By using

Eq. (1), the $\Delta\rho_{xx}/\rho_{xx}$-$H$ curve can be fitted with a high precision [Fig. 1(d)]. From this fitting, the obtained effective spin lifetime τ is 1.94 ps, and the maximal $(\Delta\rho/\rho)_{H\to\infty}$ is 1.2×10^{-4}, which is in accordance with the theoretical estimation for edge spin accumulation–induced HMR [24]. Normalized HMR at 9 T can reach 6.7×10^{-5}, which is more than one order of magnitude larger than previous report in Si-SiO_2/Ta [28]. Compared to the previous method of the lift-off process followed by film deposition, in our work, the film is deposited first with an *in situ* pre-etching process, and then the Hall bar geometry is fabricated. Our method promises a much cleaner and sharper interface between films and substrates, which is critical to the quality of the Pt film and the edge spin accumulation. Figure 1(e) shows the R-H curves with magnetic field scanning from −9 to 9 T along x, y, and z directions. The maximal HMR happens when the magnetic field is along y and z directions, where $\boldsymbol{H}$ is perpendicular to $\boldsymbol{\sigma}$.

The thickness dependence of the HMR due to edge spin accumulation can be described as the following equation [28]:

$$\Delta\rho/\rho = 2\theta_{\mathrm{SH}}^2\left\{\frac{\lambda}{d}\tanh\left(\frac{d}{2\lambda}\right) - \Re\left[\frac{\Lambda}{d}\tanh\left(\frac{d}{2\Lambda}\right)\right]\right\}, \quad (2)$$

where d is the thickness of HM, $\Lambda = (\sqrt{1/\lambda^2 + i/\lambda_m^2})^{-1}$ with $\lambda_m = \sqrt{D\hbar/g\mu_{\mathrm{B}}B}$, and electron diffusion coefficient $D = 6.0 \times 10^{-6}\ \mathrm{m^2 s^{-1}}$ in a previous report [28]. When we changed the thickness of Pt from 3 to 20 nm, we kept the angular dependences of HMR the same, while the normalized HMR $\Delta\rho_{xx}/\rho_{xx}$ decreases with increasing the thickness, as seen in Fig. 2(a). By fitting the thickness dependence of normalized HMR with Eq. (2) [Fig. 2(b)], we obtained $\theta_{\mathrm{SH}} = 0.12$ and $\lambda = 0.88$ nm. The experimental variation and the possible weak thickness dependence of D, θ_{SH}, and λ could contribute to the uncertainty for the fitting result. It is worth noticing that θ_{SH} and λ in our work come from the intrinsic Pt without any other FM, which are thus free from the interfacial spin mixing conductance between FM and HM [25–27]. Therefore, the obtained intrinsic spin Hall angle in our work should be the upper bound, which is in accordance with the relative larger values by spin pumping measurement [14,31,32].

Figure 3 shows the temperature dependence of the normalized ADMR between 10 and 300 K. HMR slightly increases with decreasing the temperature from 300 to 50 K, and the increasing spin relaxation time at lower temperature contributes to this increase. A sharp increase of ADMR appears below 50 K, which comes from the weak antilocalization (WAL) in thin films with strong SOC at low temperature. The nonlinear R-T property of Pt (inset in Fig. 3) below 50 K and the increasing resistance from 10 to 2 K also confirm the existence of WAL, which would contribute to an additional MR at low temperature [33–35].

Next, our data focus on GGG/YIG/Pt system. The cross-sectional morphology of the GGG/YIG and YIG/Pt interfaces was characterized by a high-resolution transmission electron microscope (HRTEM). From the GGG/YIG interface in Fig. 4(a), we can see that the high-quality YIG crystal epitaxially grows along the (111)-directional GGG substrate, and selected area electron diffraction (SAED) patterns from GGG and YIG areas respectively also show the coherent lattice

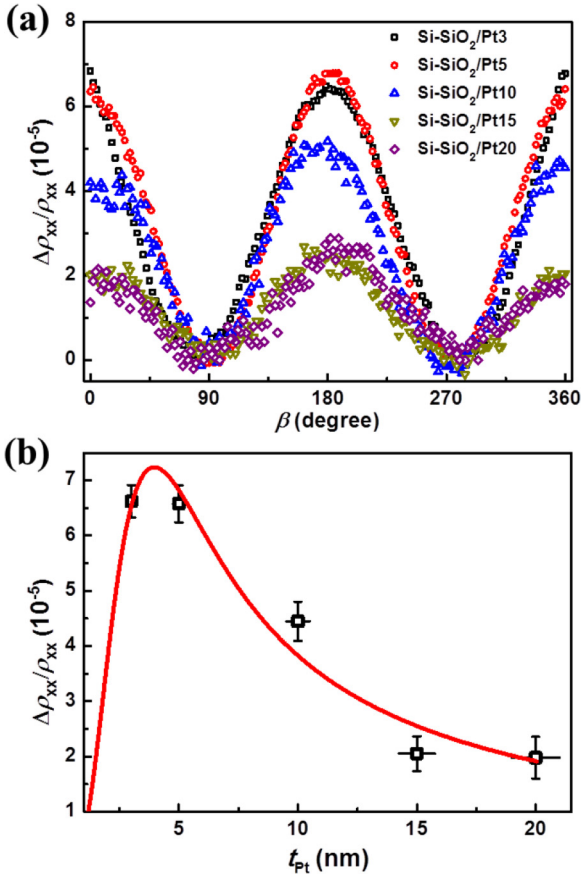

FIG. 2. (a) The normalized ADMR curves measured in Si-SiO_2/Pt (t nm) t = 3, 5, 10, 15, and 20 at a 9-T magnetic field at 300 K. (b) The thickness dependence of normalized HMR, which is obtained from the amplitude of ADMR, and the fitting curve from Eq. (2) (red line).

relationship. The well-defined YIG/Pt interface is shown in Fig. 4(b), which is crucial to the interfacial spin current transport between YIG and Pt. Figure 4(c) shows the flat

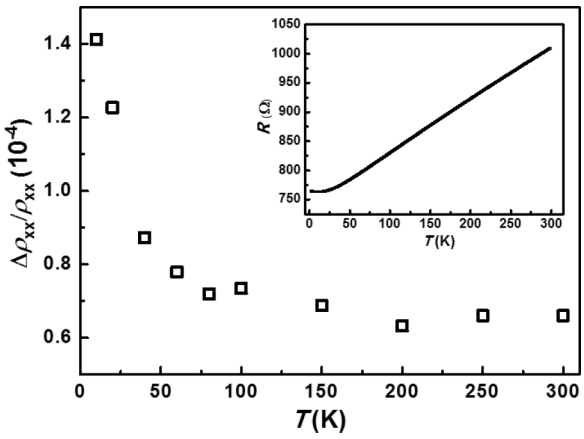

FIG. 3. The temperature dependence of normalized ADMR between 10 and 300 K measured in Si-SiO_2/Pt (5 nm) at a 9-T magnetic field, and the inset shows the temperature dependence of the resistance of Pt (2–300 K).

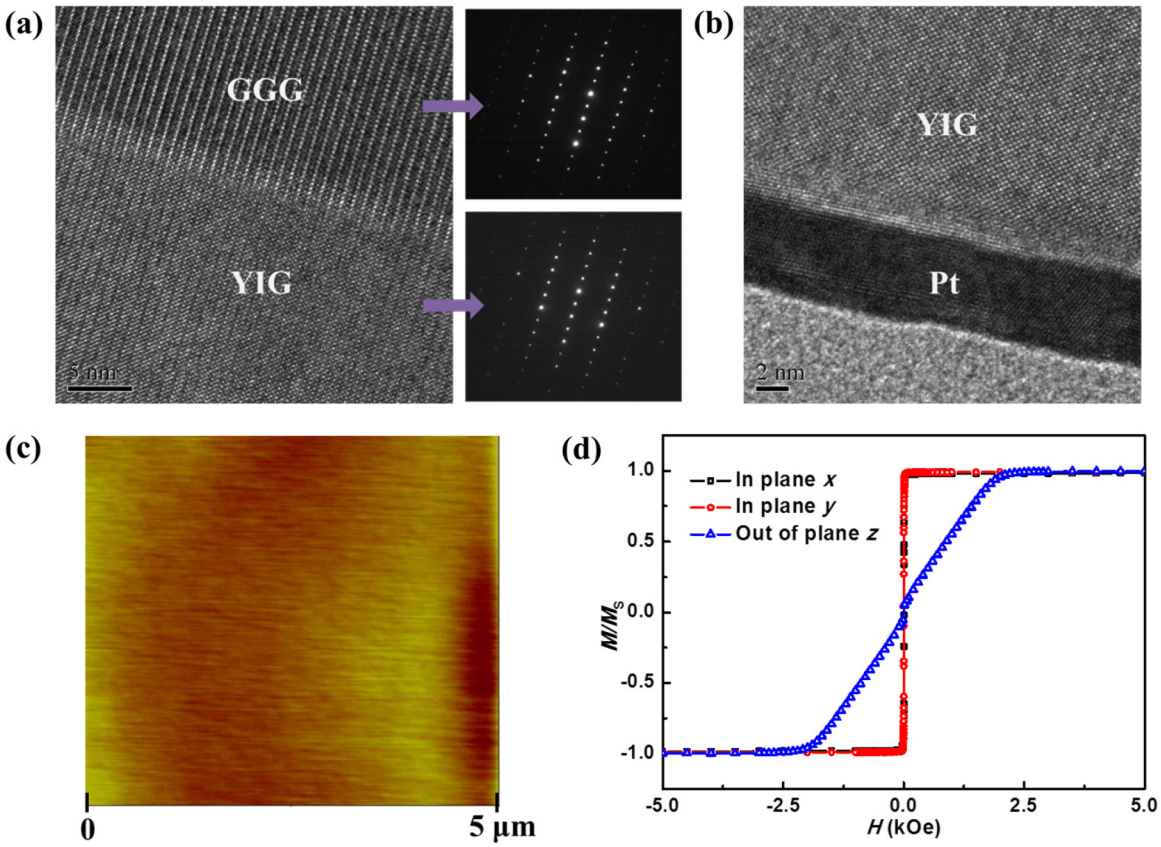

FIG. 4. (a) HRTEM results of the GGG/YIG interface; insets show the SAED patterns of GGG and YIG areas respectively. (b) HRTEM results of the YIG/Pt interface. (c) Surface topography of the YIG/Pt film measured by atomic force microscope (AFM). (d) The magnetic field dependences of the magnetization of YIG with field along x, y, and z directions.

surface of YIG/Pt film and the roughness is about 0.7 nm. Normalized M-H loops with magnetic field along x, y, and z directions show the in-plane magnetic anisotropy of the YIG film, and the calculated saturation magnetization M_S of YIG is 140 emu/cc, as seen in Fig. 4(d).

SMR, as a typical effect in YIG/Pt system, must be considered in this sample. In SMR theory [21–23], the charge current along the y direction in Pt will generate a spin current along the z direction with x-directional spin polarization by SHE. Then a part of the spin current flows to the YIG/Pt interface, which can be absorbed or reflected by YIG, and the amount of spin current absorption or reflection depends on the orientation of the YIG magnetization $\boldsymbol{M}$ with respect to the spin polarization $\boldsymbol{\sigma}$; thus the additional induced charge current due to ISHE could be controlled by the magnetization of YIG, which would influence the resistance of Pt. For HMR, spin precession by magnetic field can destroy both injected and reflected spin current, which would induce an increase of the resistance of Pt via ISHE.

The SMR contribution only depends on the magnetization $\boldsymbol{M}$ of YIG, while HMR comes from the magnetic field $\boldsymbol{H}$. SMR and HMR share the same angular dependence, so ADMR will be enhanced at high magnetic field due to the coexistence of SMR and HMR. We attribute the ADMR at 1 T dominantly to the SMR contribution [Fig. 5(a)], because the magnetization $\boldsymbol{M}$ of YIG will be saturated at 1 T in any direction. With increasing the magnetic field from 1 to 9 T during the ADMR measurement, we find the amplitude of ADMR has an increase, which shows the HMR contribution, as seen in Fig. 5(b). Except the SMR contribution at 1 T, normalized HMR $\Delta\rho_{xx}/\rho_{xx}$ obtained from the amplitude of ADMR can also be fitted by Eq. (1), as shown in Fig. 5(c). The effective spin lifetime τ is 0.61 ps, and the maximal $(\Delta\rho/\rho)_{H\to\infty}$ is 9.5×10^{-4}. The normalized HMR obtained from the difference value between 9 and 1 T is 2.0×10^{-4}, which is two times larger than that in Si-SiO_2/Pt. As for scanning the magnetic field, apart from the SMR contribution at low magnetic field (less than 5 kOe), HMR is observed with field along y and z directions [Fig. 5(d)], where $\boldsymbol{H}$ is perpendicular to $\boldsymbol{\sigma}$. While for parallel $\boldsymbol{H}$ along x direction, HMR is suppressed.

In order to get the temperature dependence of HMR, we measured the temperature-dependent ADMR at 1 and 9 T respectively, and obtained the HMR contribution from the difference value [Fig. 6]. We attribute the ADMR at 1 T to the SMR contribution, and SMR shows the similar temperature dependence with previous report [36]. While for HMR, the temperature dependence in the YIG/Pt sample is different from that in Si-SiO_2/Pt sample. With decreasing the temperature, HMR in YIG/Pt gradually decreases, while in Si-SiO_2/Pt it has a slight increase until 50 K. This can be understood as follows: The spin current transport across the YIG/Pt interface depends on the spin conversion efficiency between spins in Pt and magnons in YIG. The magnon absorption and

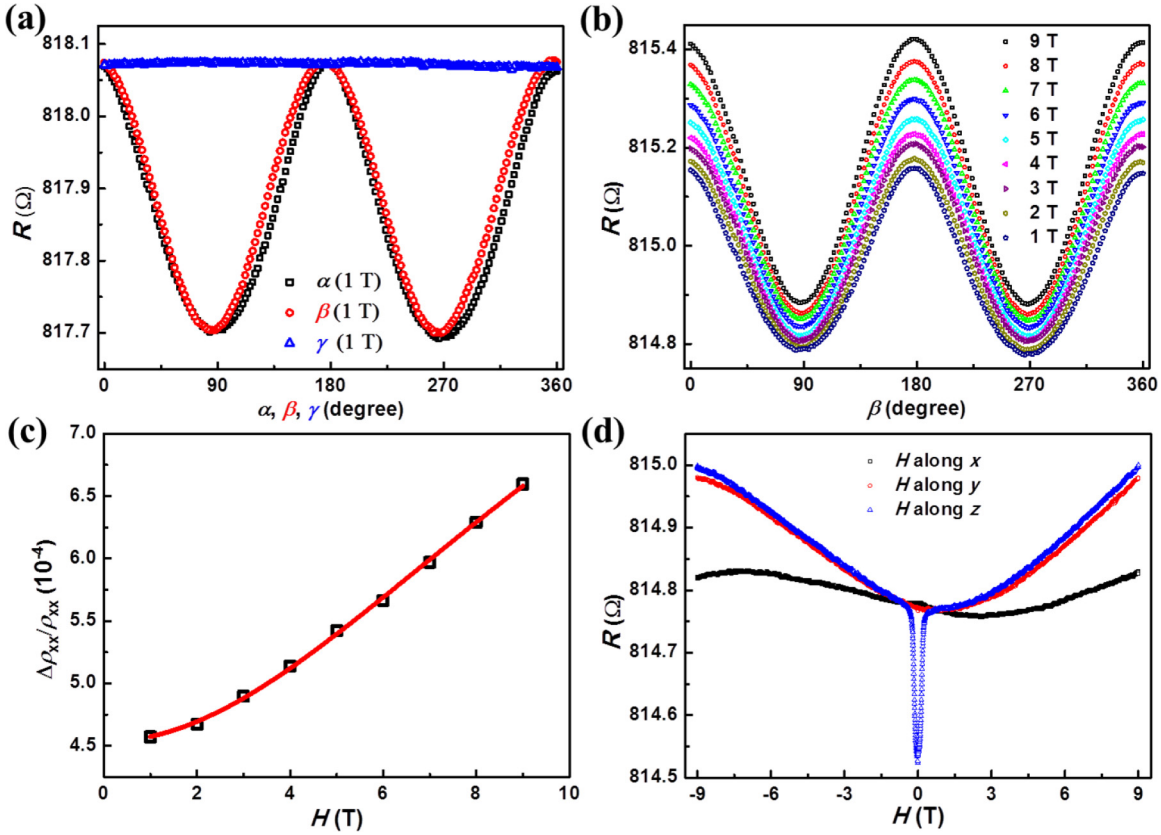

FIG. 5. Panels (a)–(d) were measured in YIG/Pt(5 nm) sample at 300 K. (a) ADMR measurements with sample scanning in three planes (α, β, γ) at a 1-T magnetic field, which mainly comes from the SMR contribution. (b) ADMR measurements at the magnetic field from 1 to 9 T. (c) The magnetic field dependence of normalized HMR, which is obtained from the amplitude of ADMR curves, and the fitting curve from Eq. (1) (red line). (d) *R*-*H* curves with magnetic field scanning from −9 to 9 T along *x*, *y*, and *z* directions.

emission rates scale with the equilibrium number of magnons, where thermal energy $k_B T$ is needed to excite the equilibrium number of magnons. As a result, the spin conversion efficiency decreases with decreasing the temperature, which leads to a decreasing interfacial spin current and an induced decreasing HMR [37–39]. In addition, the magnetic proximity effect (MPE) [21] should be enhanced at lower temperature, which is not applicable in our system.

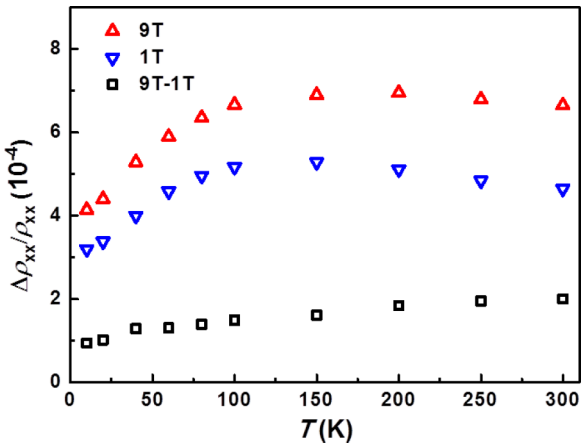

FIG. 6. The temperature dependence of normalized ADMR between 10 and 300 K measured in YIG/Pt (5 nm) at the magnetic field of 1 and 9 T respectively. In order to show the temperature dependence of the HMR contribution, we calculated the difference value between 9 and 1 T.

The effective spin lifetime τ is a combined effect of spin relaxation time τ_S and spin diffusion time τ_d [24,40]:

$$\frac{1}{\tau} = \frac{1}{\tau_S} + \frac{1}{\tau_d},$$

and the effective spin lifetime τ in YIG/Pt (0.61 ps) is much shorter than that in Si-SiO_2/Pt (1.94 ps). Because HMR in Si-SiO_2/Pt only comes from the spin precession of edge spin accumulation, and the additional interfacial spin current also plays a role in YIG/Pt besides of edge spin accumulation, we suppose that the shorter effective spin lifetime in YIG/Pt is probably related to the spin diffusion process of this interfacial spin current. For the temperature dependence, the spin conversion efficiency in the YIG/Pt interface for interfacial spin current transport dominates the temperature dependence of HMR, which decreases with decreasing the temperature, while for edge spin accumulation in Si-SiO_2/Pt, the increasing spin relaxation time at lower temperature results in an increasing HMR.

In summary, HMR in Si-SiO_2/Pt and YIG/Pt was investigated systematically. After careful optimization of deposition

conditions, HMR of a single Pt layer on Si-SiO_2 at room temperature was observed, and the intrinsic spin diffusion length (0.88 nm) and spin Hall angle (0.12) of Pt were obtained by fitting the thickness dependence. Two microscopic mechanisms of HMR were discussed: spin precession of edge spin accumulation and interfacial spin current respectively. Spin relaxation governs the HMR from edge spin accumulation, while spin diffusion and spin conversion play important roles in the HMR from interfacial spin current. This work experimentally reports a type of magnetoresistance in thin films with strong SOC and provides a way to quantify the intrinsic spin transport parameters.

This work was supported by the Ministry of Science and Technology of China [Grants No. 2014AA032904 and No. 2011YQ120053], the National Natural Science Foundation of China [Grants No. 11434014 and No. 11404382], and the Chinese Academy of Sciences [Grant No. XDB07030200].

[1] A. Manchon, H. C. Koo, J. Nitta, S. M. Frolov, and R. A. Duine, Nat. Mater. **14**, 871 (2015).
[2] T. Kuschel and G. Reiss, Nat. Nanotechnol. **10**, 22 (2015).
[3] J. E. Hirsch, Phys. Rev. Lett. **83**, 1834 (1999).
[4] Y. K. Kato, R. C. Myers, A. C. Gossard, and D. D. Awschalom, Science **306**, 1910 (2004).
[5] O. Mosendz, J. E. Pearson, F. Y. Fradin, G. E. W. Bauer, S. D. Bader, and A. Hoffmann, Phys. Rev. Lett. **104**, 046601 (2010).
[6] E. Saitoh, M. Ueda, H. Miyajima, and G. Tatara, Appl. Phys. Lett. **88**, 182509 (2006).
[7] S. O. Valenzuela and M. Tinkham, Nature (London) **442**, 176 (2006).
[8] T. Kimura, Y. Otani, T. Sato, S. Takahashi, and S. Maekawa, Phys. Rev. Lett. **98**, 156601 (2007).
[9] R. Karplus and J. M. Luttinger, Phys. Rev. **95**, 1154 (1954).
[10] J. Smit, Physica (Amsterdam) **24**, 39 (1958).
[11] L. Berger, Phys. Rev. B **2**, 4559 (1970).
[12] H. L. Wang, C. H. Du, Y. Pu, R. Adur, P. C. Hammel, and F. Y. Yang, Phys. Rev. Lett. **112**, 197201 (2014).
[13] W. Park, D. V. Baxter, S. Steenwyk, I. Moraru, W. P. Pratt, and J. Bass, Phys. Rev. B **62**, 1178 (2000).
[14] H. J. Jiao and G. E. W. Bauer, Phys. Rev. Lett. **110**, 217602 (2013).
[15] J. Slonczewski, J. Magn. Magn. Mater. **159**, L1 (1996).
[16] B. Ozyilmaz, A. D. Kent, D. Monsma, J. Z. Sun, M. J. Rooks, and R. H. Koch, Phys. Rev. Lett. **91**, 067203 (2003).
[17] J. C. Sankey, Y. T. Cui, J. Z. Sun, J. C. Slonczewski, R. A. Buhrman, and D. C. Ralph, Nat. Phys. **4**, 67 (2008).
[18] L. Liu, C. F. Pai, Y. Li, H. W. Tseng, D. C. Ralph, and R. A. Buhrman, Science **336**, 555 (2012).
[19] I. M. Miron, K. Garello, G. Gaudin, P. J. Zermatten, M. V. Costache, S. Auffret, S. Bandiera, B. Rodmacq, A. Schuhl, and P. Gambardella, Nature (London) **476**, 189 (2011).
[20] Y. Tserkovnyak, A. Brataas, and G. E. W. Bauer, Phys. Rev. Lett. **88**, 117601 (2002).
[21] S. Y. Huang, X. Fan, D. Qu, Y. P. Chen, W. G. Wang, J. Wu, T. Y. Chen, J. Q. Xiao, and C. L. Chien, Phys. Rev. Lett. **109**, 107204 (2012).
[22] H. Nakayama, M. Althammer, Y. T. Chen, K. Uchida, Y. Kajiwara, D. Kikuchi, T. Ohtani, S. Geprags, M. Opel, S. Takahashi, R. Gross, G. E. W. Bauer, S. T. B. Goennenwein, and E. Saitoh, Phys. Rev. Lett. **110**, 206601 (2013).
[23] H. Wu, Q. T. Zhang, C. H. Wan, S. S. Ali, Z. H. Yuan, L. You, J. Wang, Y. Choi, and X. F. Han, IEEE Trans. Magn. **51**, 4100104 (2015).
[24] M. I. Dyakonov, Phys. Rev. Lett. **99**, 126601 (2007).
[25] M. Weiler, M. Althammer, M. Schreier, J. Lotze, M. Pernpeintner, S. Meyer, H. Huebl, R. Gross, A. Kamra, J. Xiao, Y. T. Chen, H. J. Jiao, G. E. W. Bauer, and S. T. B. Goennenwein, Phys. Rev. Lett. **111**, 176601 (2013).
[26] Z. Qiu, K. Ando, K. Uchida, Y. Kajiwara, R. Takahashi, H. Nakayama, T. An, Y. Fujikawa, and E. Saitoh, Appl. Phys. Lett. **103**, 092404 (2013).
[27] P. Deorani and H. Yang, Appl. Phys. Lett. **103**, 232408 (2013).
[28] S. Velez, V. N. Golovach, A. Bedoya-Pinto, M. Isasa, E. Sagasta, M. Abadia, C. Rogero, L. E. Hueso, F. S. Bergeret, and F. Casanova, Phys. Rev. Lett. **116**, 016603 (2016).
[29] L. Gtai and I. Mojzes, Appl. Phys. Lett. **26**, 325 (1975).
[30] W. T. Masselink, W. Kopp, T. Henderson, and H. Morkoc, IEEE Electron Dev. Lett. **6**, 539 (1985).
[31] W. Zhang, V. Vlaminck, J. E. Pearson, R. Divan, S. D. Bader, and A. Hoffmann, Appl. Phys. Lett. **103**, 242414 (2013).
[32] M. Obstbaum, M. Härtinger, H. G. Bauer, T. Meier, F. Swientek, C. H. Back, and G. Woltersdorf, Phys. Rev. B **89**, 060407(R) (2014).
[33] Y. Niimi, D. Wei, H. Idzuchi, T. Wakamura, T. Kato, and Y. C. Otani, Phys. Rev. Lett. **110**, 016805 (2013).
[34] Y. Shiomi, T. Ohtani, S. Iguchi, T. Sasaki, Z. Qiu, H. Nakayama, K. Uchida, and E. Saitoh, Appl. Phys. Lett. **104**, 242406 (2014).
[35] J. Ryu, M. Kohda, and J. Nitta, Phys. Rev. Lett. **116**, 256802 (2016).
[36] S. R. Marmion, M. Ali, M. McLaren, D. A. Williams, and B. J. Hickey, Phys. Rev. B **89**, 220404(R) (2014).
[37] S. S. L. Zhang and S. Zhang, Phys. Rev. Lett. **109**, 096603 (2012).
[38] S. S. L. Zhang and S. Zhang, Phys. Rev. B **86**, 214424 (2012).
[39] H. Wu, C. H. Wan, X. Zhang, Z. H. Yuan, Q. T. Zhang, J. Y. Qin, H. X. Wei, X. F. Han, and S. Zhang, Phys. Rev. B **93**, 060403(R) (2016).
[40] Y. Araki, G. Khalsa, and A. H. MacDonald, Phys. Rev. B **90**, 125309 (2014).